*International Journal of the Korean Society of Precision Engineering Vol. 4, No. 4, July 2003.*

# 2 Dimensional Modeling of Centerless Grinding - Infeed (Plunge) Process -

Kang Kim#

School of Mechanical and Automotive Engineering, Kookmin University, Seoul, South Korea

## ABSTRACT

A computer simulation model for investigating a two-dimensional (2-D) rounding mechanism in a centerless grinding process is described. This model includes the interference phenomena and the concept of machining elasticity. Since initial contact points are used as a reference, the result of this simulation is not affected by the location of the reference circle center and the radius of the reference circle. Also, details of the machining factor are studied by using process variables (grinding wheel speed, wheel specification, workpiece speed, dressing condition, etc.). The effect of the threshold grinding force on the size of ground workpiece is investigated. For the verification of this method, simulation results are compared with the experimental work.

**Key Words** : Centerless grinding, Rounding mechanism, Machining elasticity, Threshold grinding force

## 1. Introduction

The first theoretical and quantitative research about rounding mechanisms in centerless grinding was carried out by Dall[1] in 1946. He presented mathematical relations describing irregularities at the work-rest blade and the regulating wheel contact points, and the resultant movement of the workpiece. In 1959, Yonetsu[2,3] experimentally inspected the relations of the out-of-roundness (OOR) curve for a cylindrical workpiece before and after centerless grinding by means of harmonic analysis. He also presented a theoretical formula using Fourier series to investigate the influences of centerless grinding variables on the OOR of the ground part. The concept of machining elasticity was introduced in his formula. Vasilev[4] did similar research considering only the most dominant order of Fourier harmonics of the OOR curve of the before-grinding workpiece.

In 1964, Rowe[5,6] and Barash introduced a computer simulation method for investigating the inherent accuracy of the centerless grinding process. They developed a simulation equation based on Dall's work and the concept of machining elasticity. They derived the machining elasticity parameter from the machining factor and the elasticity factor. The interference phenomena during centerless grinding were also studied. Their simulation results matched reasonably well with the experimental results. Because of its simplicity and good modeling capability, many researchers followed this model to study dynamics and stability. They investigated an interference phenomenon and called it "Interference Restriction". They included this restriction in their computer simulation method by applying a clearance condition to modify the apparent depth of cut. Their simulation results showed good agreement with the experimental work in waviness, such as the number of lobes and the relative locations of peaks and valleys. However, details of their simulation results were different from the experimental results. The maximum peak in the simulation is higher than that in the experimental work.

☞ Manuscript received: February 4, 2003 ;
Accepted: May 16, 2003
# Corresponding Author:
Email: kangkim@kookmin.ac.kr
Tel: +82-2-910-4676 ; Fax: +82-2-910-4839

The limitations and the validity of the machining elasticity were investigated by Rowe,[5-7] Barash, and Koenigsberger. The correct machining elasticity parameter was obtained by comparing experimental data with simulation results. In 1971, Hahn and Lindsay[8,9] presented an empirical equation relating the material removal rate and the process variables. Hahn[10] also presented the influence of the grinding threshold forces on size and roundness errors. They defined the material removal rate as a product of the material removal parameter and the normal grinding force.

A basic equation which governs the rounding mechanism in centerless grinding was presented by Kim[11] et al. The simulation equation was derived from the instantaneous change of the apparent depth of cut using the interference phenomena. In this paper, the concept of machining elasticity is added to the previously developed basic equation. The relationship between the grinding geometry and the waviness of the ground part is presented with this model. Also shown are the relations between grinding interference and machining elasticity, the effect of the threshold grinding force on material removal, and the contributions of the grinding variables to the rounding mechanism.

## 2. Grinding Geometry and 2D Modeling

Fig. 1 shows the configuration of the centerless grinding geometry where $\theta$ is the angle of rotation ($\angle O_gOX$) between the initial reference line OX on the workpiece and the grinding wheel contact normal shown as $OO_g$; $\alpha$ is the angle ($\angle O_gOB$) between the line $OO_g$ and the normal line OB of the work-rest blade surface ; $\beta$ is the supplementary angle ($\pi - \angle O_gOO_r$) between the line $OO_r$ connecting the workpiece center and the regulating wheel center and the line $OO_g$; $\gamma$ is the top angle of the work-rest blade; $D_g$ is the grinding wheel diameter; and $D_w$ is the workpiece diameter. The reference line OX coincides with the line $OO_g$ at the beginning of grinding. The workpiece slides on top of the work-rest blade. Workpiece rotation is governed by the regulation wheel, and the cutting action is performed by the grinding wheel.

The American National Standard[12] describes four ways of defining the center of a circle: minimum radial separations (MRS), least squares circle (LSC), maximum inscribed circle (MIC), and minimum circumscribed circle (MCC). Among these, only LSC can be defined analytically. To simulate the rounding mechanism during centerless grinding, it is necessary to define the coordinate system of the workpiece and the grinding machine. In previous works, a reference circle was defined for the simulation. However, using a different definition of the center of a circle results in a different depth of cut and the simulated final workpiece shape will be significantly different.

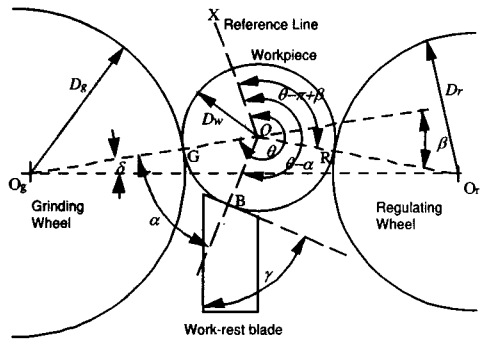


Fig. 1 Centerless grinding geometry

In this work, $r(\theta)$ is defined as the distance from any reference center, O, in the workpiece to the periphery of the workpiece at angle $\theta$ from the reference line OX. When the irregularities of the workpiece arrive either at the work-rest blade or at the regulating wheel, the workpiece will be displaced, and the apparent depth of cut at the grinding wheel contact point will be changed. Also, infeed motion increases the apparent depth of cut as shown in Fig. 2 and $X(\theta)$ is the magnitude of the infeed motion at $\theta$.

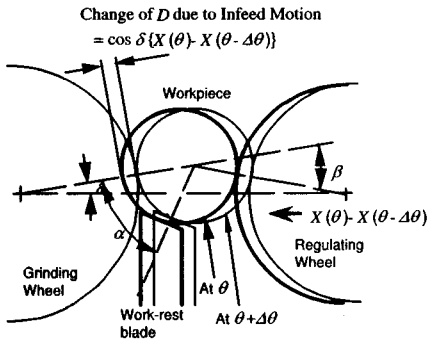


Fig. 2 Change of apparent depth of cut

The apparent depth of cut at the grinding wheel contact point can be expressed as a sum of the change of the infeed motion and the effects of the irregularities at the work-rest blade contact point, regulating wheel contact point, and grinding wheel contact point.If there is no interference restriction, the workpiece may contact tangentially with the work-rest blade, the regulating wheel, and grinding wheel at $r(\theta-\alpha)$, $r(\theta-\pi+\beta)$, and $r(\theta)$, respectively. However, in practice, the contact points do not coincide with these tangent points because of the irregularity of the workpiece. Furthermore, the material removal rate is affected by the duration of contact at the grinding wheel contact zone. When the angular displacement difference between the actual work-rest blade contact point and the ideal contact point, $r(\theta-\alpha)$, is $\zeta_\theta$, and the angular displacement difference between the actual regulating wheel contact point and the ideal contact point, $r(\theta-\pi+\beta)$, is $\xi_\theta$, the apparent depth of cut at one of the feasible grinding wheel contact points, which deviates $\eta$ from the ideal contact point angularly, $D(\theta, \eta)$, can be expressed as[11]

$$\begin{aligned} D(\theta,\eta) = D(0,0) &+ \cos\delta\{X(\theta)-X(0)\} \\ &- \frac{\sin\beta}{\sin(\alpha+\beta)}\{\cos(\zeta_\theta)r(\theta-\alpha+\zeta_\theta) \\ &- \cos(\zeta_0)r(-\alpha+\zeta_0)\} \\ &+ \frac{\sin\alpha}{\sin(\alpha+\beta)}\{\cos(\xi_\theta)r(\theta-\pi+\beta+\xi_\theta) \\ &- \cos(\xi_0)r(-\pi+\beta+\xi_0)\} \\ &+ \{\cos(\eta)r(\theta+\eta)-r(-2\pi)\} \end{aligned} \quad (1)$$

It should be noted that the negative of the last term in equation (1), $-\{\cos(\eta)r(\theta+\eta)-r(-2\pi)\}$, is the total true depth of cut accumulated at $\theta+\eta$.

The elastic deflection of the system is initiated at the peripheral point which has the maximum apparent depth of cut. If $\eta$ is the angular displacement difference between the point which has a maximum apparent depth of cut, $D(\theta, \eta_{max})$ and ideal contact point, $r(\theta)$, the deflection of the system, $x(\theta)$, is

$$x(\theta) = \frac{F_n(\theta)}{K_e} = \cos(\eta_{max})\{D(\theta, \eta_{max}) - L(\theta, \eta_{max})\} \quad (2)$$

where $K_e$ is the elasticity factor of the machine system, $F_n(\theta)$ is the normal grinding force, and $L(\theta, \eta_{max})$ is the true depth of cut at the point which has the maximum apparent depth of cut.

If $r(\theta, \eta_k)$ is the one of the grinding wheel contact points, the true depth of cut, $L(\theta, \eta_k)$, with its corresponding $D(\theta, \eta_k)$ is

$$L(\theta,\eta_k) = \frac{\cos(\eta_k)D(\theta,\eta_k) - x(\theta)}{\cos(\eta_k)} \quad (3)$$

$$(when\ \cos(\eta_k)D(\theta,\eta_k) \geq x(\theta))$$

When $\cos(\eta_k)D(\theta, \eta_k)$, is less than the deflection of the system, $x(\theta)$, material removal will be zero.

If the normal grinding force is lower than the threshold force, rubbing or plowing occurs. Above this threshold force, the material removal rate is proportional to the normal grinding force[13]. The relationship between the material removal rate and the normal grinding force is given by:

$$Z_w = (F_n - P_0)\,\Lambda_w \quad (4)$$

where $Z_w$, $P_0$, and $\Lambda_w$ are the material removal rate, the threshold grinding force, and material removal parameter, respectively (Fig. 3).

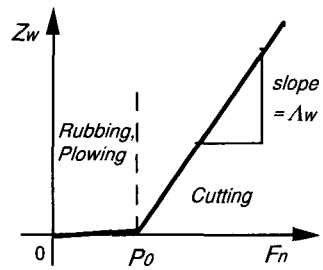


Fig. 3 Relationship between material removal rate and normal grinding force

The material removal rate can be expressed as

$$Z_w = V_w w\left\{\sum_{for\ all\ k} L(\theta,\eta_k)\right\} \quad (5)$$

where $V_w$ and $w$ are the workpiece surface speed and workpiece length, respectively. From equations (4) and (5), the normal grinding force can be formulated as a linear function of the true depth of cut:

$$F_n(\theta) = \frac{Z_w}{\Lambda_w} + P_0$$
$$= \frac{V_w w}{\Lambda_w} \sum_{for\ all\ k} \{\cos(\eta_k) L(\theta, \eta_k)\} + P_0$$
$$= K_m \sum_{for\ all\ k} \{\cos(\eta_k) L(\theta, \eta_k)\} + P_0 \quad (6)$$

where $K_m$ is the machining factor.

If the workpiece material is easy to grind (not a high temperature alloy), Lindsay's empirical equation of $\Lambda_w$[8] can be modified for the centerless grinding process as follows.

$$\Lambda_w = \frac{(7.81\times10^{-7})}{2} \frac{\left(\frac{V_w}{V_g}\right)^{0.158} \left(1+\frac{2C}{3l}\right) l^{0.58} V_g}{\left(\frac{D_w D_g}{D_w + D_g}\right)^{0.14} (Vol)^{0.47} d^{0.13} (R_c)^{1.42}} \quad (7)$$

where $\Lambda_w$ is the material removal parameter ($m^3$/sec/N); $V_g$ is the grinding wheel surface speed (m/sec); $V_w$ is the workpiece surface speed (m/sec); $C$ is the dressing compensation (m); $l$ is the dressing lead (m/revolution); $d$ is the abrasive grain diameter (m); $Vol$ is the volume percent of bond material in the wheel; and $R_c$ is the Rockwell C scale hardness of the workpiece. The abrasive grain diameter, $d$, can be approximately expressed as a function of the abrasive mesh number, $M$, as follows[14]:

$$d = 0.028\, M^{-1.1} \quad (8)$$

From equations (6) through (8), we get

$$K_m = (1.61\times10^6) \frac{\left(\frac{D_w D_g}{D_w + D_g}\right)^{0.14} (Vol)^{0.47} (R_c)^{1.42} \left(\frac{V_w}{V_g}\right)^{0.842} w}{\left(1+\frac{2C}{3l}\right) l^{0.58} M^{0.143}} \quad (9)$$

If there are positive $x(\theta)$ and $L(\theta,\eta_k)$, which satisfy equations (2), (3), and (6) simultaneously, the actual material removal can happen. Therefore, if a peripheral point, $r_{old}(\theta+\eta_k)$, is ground at rotation $\theta$, then this peripheral point just after this instantaneous grinding, $r_{new}(\theta+\eta_k)$, can be expressed as

$$r_{new}(\theta+\eta_k) = r_{old}(\theta+\eta_k) - L(\theta, \eta_k) \quad (10)$$

## 3. Experiment

The experimental details are given in Table 1. The pre-grinding shape of the specimens in this experiment was that of a partially flat cylindrical hollow bar, as shown in Fig. 4. The initial roundness error of the specimens, except the flat area, was within 2μm, and the depth of flat was 66μm. This shape is easy to control and includes all orders of harmonics below the fortieth with the largest amplitudes obtained for the lowest orders[6]. It is useful to find any effect of the grinding variables on a certain order of waviness.

Table 1 Experimental condition

| | | |
|---|---|---|
| Grinding machine | Cincinnati CINCO 15 | |
| Grinding Wheel | 97A 80 J6 VFM<br>ϕ584.2 × 101.6 × 304.8 mm hole | |
| Regulating Wheel | A80 R2<br>ϕ322.5 × 101.6 × 127.0 mm hole | |
| Work-rest blade | Sintered Carbide | |
| Specimen | Steel ( $H_{RC}$= 62 ) | |
| Geometric set-up | α = 57.9°, β = 5.9°, γ = 60° | |
| R.W. speed<br>G.W. speed | 20 rpm<br>1200 rpm | |
| Dressing traverse rate | 53 μm/rev. ( 2.5"/min )<br>( 4 passes 25.4 μm (0.001") depth ) | |
| | CASE 1 | CASE 2 |
| Total infeed | 77 μm | 210 μm |
| Infeed time | 7.5 sec (35 rev.) | 17.5 sec (82 rev.) |
| Spark out time | 6.0 sec (28 rev.) | 6.0 sec (28 rev.) |

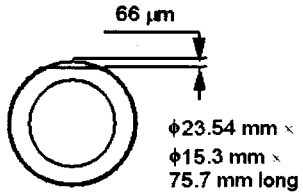


Fig. 4 Before-grinding shape of specimen

To verify the simulation method, these specimens were ground under two different conditions. In the first case, the infeed time was limited to 7.5 seconds so that the flat area was partially unground (Fig. 5). In the second case, the infeed time was 17.5 seconds and the material was removed from all over the surface (Fig. 6).

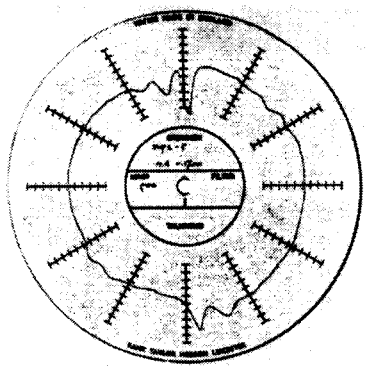

Fig. 5 Experimental result (Infeed: 77μm, 1 scale=5μm)

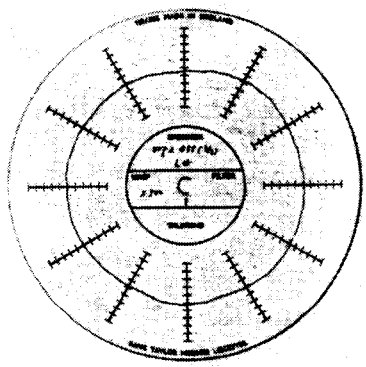

Fig. 6 Experimental result (Infeed: 210μm, 1 scale=5μm)

The roundness profiles of the ground specimens were measured on the Talyrond 100 machine from Rank Taylor Hobson.

## 4. Simulation

In the computer simulations, the workpiece was divided into 360 equi-spaced radii. The magnitude of these radii at any given moment defined the shape of the workpiece.

The initial contact point between the workpiece and the grinding wheel was determined by finding the maximum displacement at the grinding wheel contact in one revolution using the following equation:

$$MAX\left[-\frac{\sin\beta}{\sin(\alpha+\beta)}r(\phi-\theta)+\frac{\sin\alpha}{\sin(\alpha+\beta)}r(\phi-\pi+\beta)+r(\phi-2\pi)\right] \quad (0\le\phi\le 2\pi) \tag{11}$$

At each increment of rotation, a new workpiece position and ideal contact points at the regulating wheel and work-rest blade are found, and the real contact points are searched. The apparent depth of cut, $D$, of each feasible grinding wheel contact point, which is engaged in this wheel at this instant, is calculated. The maximum apparent depth of cut, $D_{max}$, is found among the $D$s. Then, the maximum true depth of cut, $L_{max}$, corresponding to $D_{max}$, is assumed as 0, and the deflection force, $F_e$, is calculated from $D_{max}$ and $L_{max}$ initially. From the geometric relation between $D_{max}$, and each $D$, $L$ of each $D$ is determined, and the grinding force, $F_n$, is also calculated initially. Then, $F_e$ is compared with $F_n$, and if the difference between these forces is larger than a pre-set error bound, ε, $L_{max}$ is increased by a pre-set incremental step size, $\Delta L$. This force calculation routine is repeated till this force difference reaches ε. Then, each $r$ in the grinding wheel contact zone is renewed by subtracting corresponding $L$ from the old $r$. In every 360 steps, the number of rotations is increased by 1, and this simulation is terminated when the number of rotations is larger than the specified rotations.

The first computer simulation was carried out under the same conditions as Rowe, Barash, and Koenigsberger's experiment[6]. $C/l$, $R_c$, and $P_0$ were assumed as 0.1, 50, and 45N, respectively. The calculated machining factor, $K_m$, from equation (9) was 151MN/m, and the elasticity factor ($K_e$), 16MN/m, was cited from the reference 15. To verify that the proposed model is independent of the reference circle center, three different centers were used as references for the simulation (LSC, MIC, and MCC centers) as shown in Fig. 7.

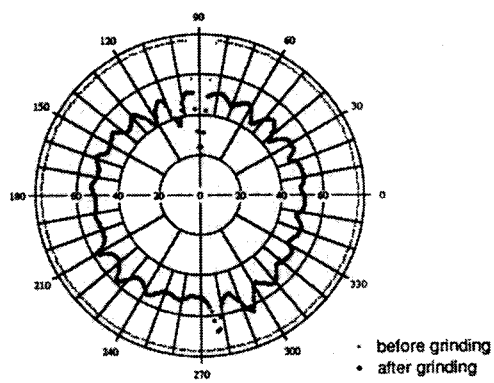


Fig. 7 Simulation result using three different centers (unit: μm)

The second and the third simulations were performed using the MCC center under the Case 1 condition and Case 2 condition, respectively. The threshold grinding force, $P_0$, 210N was quoted from the reference 16, and the machining factor, $K_m$, was calculated as 195.5MN/m with equation (9). The elasticity factor, $K_e$, 20MN/m, was cited from the reference 15. The simulation results of Case1 and Case 2 are also presented in Figs. 8 and 9, respectively. The angular range corresponding to the initial flat width was ±7°. Thus, for the simulations using the interference model, the peripheral points within the ranges $\theta-\alpha\pm7°$ and $\theta-\pi+\beta\pm7°$ were checked at every $\theta$ to find the true contact points at the work-rest blade and the regulating wheel. In the same way, the peripheral points within the range $\theta\pm7°$ were considered as feasible grinding wheel contact points.

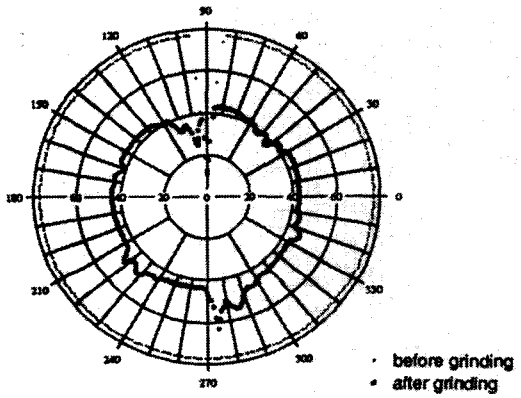


Fig. 8 Simulation result (Case 1) (unit: μm)

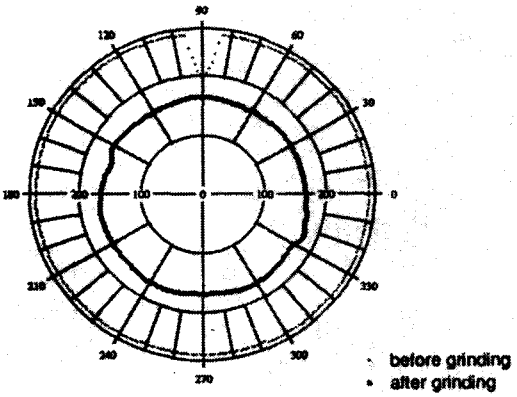


Fig. 9 Simulation result (Case 2) (unit: μm)

## 5. Discussions

The simulation results using three different centers were identical (Fig. 7). It is shown that this model is not affected by the coordinate system. The simulation result shows that the number of lobes and the angular displacement of peaks and valleys are similar to what are shown in the corresponding experimental work done by Rowe[5] and Barash. The number of lobes is about $\pi/\beta$, and the angular displacement difference between a peak and the corresponding valley is $\pi-\beta$. This relationship between the angle $\beta$ and the waviness of the roundness profile is clearly shown when the flat area of workpiece is partially unground (Figs. 5, 7, 8).

Figs. 7, 8, and 9 show the results of the simulation including the interference model. Under these restrictions, the points around the peak are ground longer in each revolution of the workpiece. These points are ground more without any effect on the points around the maximum valley. Thus, the simulation result of Case 1 shows that the height of the maximum peak was reduced. As a result of this reduction, the error at the second maximum valley was also cleared, and this error correction propagated all over the workpiece periphery.

The effects of a different dressing lead and the grinding wheel surface conditions can be found from the machining elasticity model. When the dressing traverse rate was doubled, the machining factor was reduced by 33%. Accordingly, the material removal rate is increased. This trend is again consistent with the reported values[6]. The threshold grinding force divided by the elasticity factor is the minimum apparent depth of cut which can be ground. Normally, this force is larger for hard materials than that for soft materials. So the effect of this force on the after-ground size is easily found in the result of Case 1 (Fig. 8). In Case 1, the total infeed was 77 μm and the difference in diameters before and after grinding was 68 μm. The difference between these two values, 9 μm, is the corresponding minimum apparent depth of cut due to the threshold grinding force. The calculated minimum apparent depth of cut was indeed 10.5 μm.

If the infeed rate is constant, the process reaches the steady state apparent depth of cut and true depth of cut after an initial 10 revolutions. All simulation results showed that the average true depth of cut is equal to the infeed rate during this steady state. This is consistent

with the published research result[14]. All these show that this model matched well with the centerless infeed grinding process not only in global shape generation but also in details of the rounding mechanism.

## 6. Conclusions

A computer simulation method for investigating a 2-D rounding mechanism in centerless grinding was developed from the concepts of machining elasticity and interference phenomena. The instantaneous change of the apparent depth of cut was represented as a function of the grinding geometry, infeed condition, and workpiece geometry. A machining elasticity parameter model was also developed to study the effect of the grinding variables. The final geometry of the ground part can be simulated with these models. For verification of this method, computer simulation was carried out and compared with the experimental data. It was shown that the current simulation model is not affected by the location of the reference point. Final out-of roundness and workpiece diameter matched very favorably with experimental data. The machining factors calculated in the current model under different grinding conditions also matched well with reported values. From this work, the effect of threshold grinding force in the centerless grinding process was also shown.

## References


1. Dall, A. H., "Rounding Effect in Centerless Grinding," Mech. Engg, Vol. 68, No. 4, pp. 325-329, Apr. 1946.
2. Yonetsu, S., "Consideration of Centerless Grinding Characteristics Through Harmonic Analysis of Out-of-Roundness Curve," Proc. Fujihara Memorial Faculty of Engineering, Keio Univ., Vol. 12, No. 47, pp. 8-26, 1959.
3. Yonetsu, S., "Forming Mechanism of Cylindrical Work in Centerless Grinding," Proc. Fujihara Memorial Faculty of Engineering, Keio Univ., Vol. 12, No. 47, pp. 27-45, 1959.
4. Vasilev, V. A., "Centerless Grinder Setting for Improving Work-piece Form Accuracy," Machines & Tooling, Vol. 51, No. 9, pp. 8-9, 1980.
5. Rowe, W. B. and Barash, M. M., "Computer Method for Investigating the Inherent Accuracy of Centerless Grinding," Int. J. MTDR, Vol. 4, No. 2, pp. 91-116, 1964.
6. Rowe, W. B., Barash, M. M., and Koenigsberger, F., "Some Roundness Characteristics of Centerless Grinding," Int. J. MTDR, Vol. 5, No. 4, pp. 203-215, 1965.
7. Rowe, W. B., "An Experimental Investigation of Grinding Machine Compliances and Improvements in Productivity," Proc. 14th Int'l Mach. Tool Des. and Res. Conf., pp. 479-486, 1973.
8. Lindsay, R. P., On the Metal Removal and Wheel Removal Parameters, Surface Finish, Geometry and Thermal Damage in Precision Grinding, Ph.D. Dissertation, Worcester Polytechnic Institute, Mass, 1971.
9. Hahn, R. S., and Lindsay, R. P., "Principle of Grinding. Part 2, The Metal Removal Parameter," Machinery, pp. 33-39, Aug. 1971.
10. Hahn, R. S., "The Influence of Threshold Forces on Size, Roundness and Contour Errors in Precision Grinding," Annals of the CIRP, Vol. 30/1, pp. 251-254, 1981.
11. Kim, K., Cylindricity Control in Precision Centerless Grinding, Technical Report, Purdue ERC for Intelligent Manufacturing Systems, pp. 28, Sep. 1992.
12. Measurement of Out-Of-Roundness, ANSI B89.3.1-1972, ASME, Reaffirmed 1979.
13. Boothroyd, G. and Knight, W. A., Fundamentals of Machining and Machine Tools 2nd ed., Marcel Dekker, Inc., pp. 292-294, 1989.
14. Malkin, S., Grinding Technology -Theory and Application of Machining with Abrasives, Ellis Horwood Limited, pp. 2, 229, 1989.
15. Reshetov, D. N. and Portman, V. T., Accuracy of Machine Tools, ASME Press, pp. 275, 1988.
16. ASM International, Metals Handbook, 9th ed., Vol. 16 Machining, pp. 422, 1989.